

# Vibrational Strong Coupling Controlled by Spatial Distribution of Molecules within the Optical Cavity

Wonmi Ahn,<sup>1</sup> Igor Vurgaftman,<sup>2</sup> Adam D. Dunkelberger,<sup>3</sup> Jeffrey C. Owrutsky,<sup>3</sup> and Blake S. Simpkins<sup>3,\*</sup>

<sup>1</sup>National Research Council Postdoctoral Associate, U.S. Naval Research Laboratory, Washington, DC 20375, United States

<sup>2</sup>Optical Sciences Division, U.S. Naval Research Laboratory, Washington, DC 20375, United States

<sup>3</sup>Chemistry Division, U.S. Naval Research Laboratory, Washington, DC 20375, United States

\*E-mail: *blake.simpkins@nrl.navy.mil*

## Supporting Information

### Contents

Analytical Treatment of Rabi Frequency for Dipoles in Resonators.

Supporting Table.

**Table S1.** Recipes used for spin-coating and baking of SOG and PMMA films.

Supporting Figures.

**Figure S1.** FTIR transmission spectrum of a bare PMMA and SOG film.

**Figure S2.** FTIR transmission spectra of Fabry-Perot cavities with variable PMMA locations within the cavity under *s*-polarization.

**Figure S3.** FTIR transmission spectra of Fabry-Perot cavities with variable PMMA locations within the cavity under *p*-polarization.

**Figure S4.** Angular dispersion curves of Fabry-Perot cavities with variable PMMA slab locations under *s*-polarization.

**Figure S5.** Cavity dispersion curves plotted versus in-plane wavevector for cavities with variable PMMA slab locations under *s*-polarization.

**Figure S6.** Angular dispersion curves of Fabry-Perot cavities with variable PMMA slab locations under *p*-polarization.

**Figure S7.** Cavity dispersion curves plotted versus in-plane wavevector for cavities with variable PMMA slab locations under  $p$ -polarization.

**Figure S8.** Data analysis for obtaining vacuum Rabi splitting values.

**Figure S9.** Dispersion curves of single and double PMMA layer cavities.

## Analytical Treatment of Rabi Frequency for Dipoles in Resonators

For a 3D-confined mode of a resonator, the Rabi splitting can be derived from the electric-dipole interaction Hamiltonian. The first step is to quantize the electric field in the mode so that it is normalized to the vacuum energy  $\hbar\omega/2$  when integrated over the cavity volume:

$$\hat{\mathbf{E}}(\mathbf{r}) = \mathbf{e}(\mathbf{r}) \sqrt{\frac{\hbar\omega |\mathbf{e}_{max}|^2}{\epsilon_0 \int (\epsilon_g + \epsilon) |\mathbf{e}(\mathbf{r})|^2 d^3r}} (\hat{a}e^{-i\omega t} + h.c.)$$

where  $\mathbf{e}(\mathbf{r})$  is the dimensionless electric-field profile for the mode in question, as obtained by solving Maxwell's equations,  $\mathbf{e}_{max}$  is the maximum value of that field (assumed to be unity in the following), and the "group" permittivity is defined as  $\epsilon_g \equiv \frac{d(\epsilon\omega)}{d\omega}$ . For wavelength-scale and multi-wavelength optical cavities, the electric-field and magnetic-field strengths are related *via* the impedance of free space divided by the index. For deeply subwavelength cavities, the  $(\epsilon_g + \epsilon)$  term is replaced by  $2\epsilon_g$  because the magnetic-field contribution to the total energy density becomes negligible. For simplicity, we will denote this term for a general cavity,  $\epsilon_t$ .

The interaction Hamiltonian in the rotating-wave approximation is given by:

$$H_{int} = \sum_{dipoles} g_d (\hat{\sigma}_d^\dagger \hat{a} + h.c.)$$

where the sum is over all the dipoles (emitters), and the effective Rabi frequency (in units of energy) for an individual (point-like) dipole at  $\mathbf{r}_d$  is defined as:

$$g_d \equiv \sqrt{\frac{\hbar\omega |\boldsymbol{\mu}(\mathbf{r}_d) \cdot \mathbf{e}(\mathbf{r}_d)|^2}{2\epsilon_0 \int \epsilon_t |\mathbf{e}(\mathbf{r})|^2 d^3r}}$$

This expression implies that the Rabi frequency can be significantly enhanced if we place the dipole at or close to the position of the maximum field or if the effective modal volume:

$$V_{eff} = \frac{\int \epsilon_t |\mathbf{e}(\mathbf{r})|^2 d^3r}{|\mathbf{e}(\mathbf{r}_d)|^2}$$

is much smaller than the diffraction-limited volume  $(\lambda/2)^3$ . The large magnitude of the Rabi frequency in this case is related to a strong Purcell effect in subwavelength cavities. The sum

over all dipoles is relevant if there is a countable number of dipoles, all oscillating in phase in response to the modal electric field.

We can also estimate the dipole-light coupling for a quasi-continuous distribution of dipoles with a fixed volume density  $N/V$ . Using the standard approach with a Primakoff-Holstein transformation of the emitter raising and lowering operators  $\hat{\sigma}_d^\dagger$  and  $\hat{\sigma}_d$  into boson operators  $\hat{b}_d^\dagger$  and  $\hat{b}_d$ , assuming a low pump rate, and constructing a collective dipole operator, we can write:

$$\hat{D}^\dagger = \sum_d \hat{b}_d^\dagger$$

In the case of deeply subwavelength or wavelength-scale cavities, the assumption of a collective dipole should be accurate, and the results should also be applicable for the relatively short cavities employed in the present experiments.

Using this approach, we can rewrite the interaction Hamiltonian as follows:

$$H_{int} = g_{col}(\hat{D}^\dagger \hat{a} + h.c.)$$

where we have defined the collective Rabi frequency,  $g_{col}$ , and transformed the sum into an integral over a continuous distribution of dipoles:

$$g_{col} = \sqrt{\frac{\hbar\omega N \int |\boldsymbol{\mu}(\mathbf{r}) \cdot \mathbf{e}(\mathbf{r})|^2 d^3r}{2\varepsilon_0 V \int \varepsilon_t |\mathbf{e}(\mathbf{r})|^2 d^3r}}$$

Now the quantity  $\boldsymbol{\mu}(\mathbf{r})$  contains the information about the distribution of the dipoles as well as their strength. It reduces to a delta function for a single dipole to remain consistent with the expressions above.

For a planar wavelength-scale cavity of length  $L$  with an active slab of thickness  $W$  (between  $z = 0$  and  $z = W$ ), the expression above reduces to:

$$g_{col} = \sqrt{\frac{\hbar\omega N\mu^2 \int_0^W |\mathbf{e}|^2 dz}{2\varepsilon_0 V \left( \int_{-L/2}^0 \varepsilon_B |\mathbf{e}|^2 dz + \int_0^W \varepsilon_t |\mathbf{e}|^2 dz + \int_W^{L/2} \varepsilon_B |\mathbf{e}|^2 dz \right)}}$$

where only the field profile and the permittivity are a function of position. For simplicity, we can assume that the permittivity outside of the active slabs does not significantly vary with frequency, and that  $\varepsilon_B \equiv n_B^2$ .

We can approximate the electric fields in the cavity by standing waves because the metal mirrors are quite reflective. For the cavity mode under the s-polarized incident field, only the electric-field component perpendicular to the cavity axis,  $\mathbf{e}_x$ , is present, whereas both  $\mathbf{e}_x$  and  $\mathbf{e}_z$  are necessary to describe the p-polarized modes. Regardless of polarization, the normalized fields of the modes of the  $\lambda/2$  cavity are given by:

$$e_x = \cos\left(\frac{\pi z}{L}\right)$$

$$e_z = \sqrt{A} \sin\left(\frac{\pi z}{L}\right)$$

The perpendicular field component is taken to vanish at the metal mirrors, which neglects the small (<100 nm) penetration depth into the mirror at the mid-IR wavelengths. The parallel component is proportional to the derivative of the perpendicular component, as demanded by Maxwell's equations inside the cavity, and peaks at the mirrors. In the free-space approximation, the constant  $A$  is given by for the p-polarized mode:

$$A = \tan^2 \left[ \sin^{-1} \left( \frac{\sin \theta_i}{n_B} \right) \right]$$

where  $\theta_i$  is the angle of incidence at resonance from outside the cavity.  $A = 0$  for the s-polarized mode.

Carrying out the integrations in our general expression and neglecting any permittivity variation in the active slab, we obtain:

$$g_{col} = \sqrt{\frac{\hbar\omega}{2\varepsilon_0 n_B^2} \frac{N\mu^2}{V} \left[ \frac{W}{L} + \frac{1-A}{1+A} \frac{\sin\left(2\pi\left(\frac{z_c}{L} + \frac{W}{2L}\right)\right) - \sin\left(2\pi\left(\frac{z_c}{L} - \frac{W}{2L}\right)\right)}{2\pi} \right]}$$

where  $z_c$  is the position of the center of the slab along the cavity axis. For a very thin slab at the center of the cavity and s-polarized modes, the expression in the brackets reduces to  $2W/L$ . The observed Rabi splitting,  $\Omega$ , is given by  $2g_{col}$ .

**Table S1.** Recipes used for spin-coating and baking of SOG and PMMA films.

|                     |             | Spin-on glass |          |          | PMMA  |
|---------------------|-------------|---------------|----------|----------|-------|
|                     |             | 315F*         | 21F*     |          | A4†   |
|                     |             |               | <i>a</i> | <i>b</i> |       |
| Ramp                | Speed (rpm) | 500           | 500      | 500      | 500   |
|                     | Time (sec)  | 4             | 4        | 4        | 4     |
| Spin                | Speed (rpm) | 2000          | 5000     | 4500     | 2700  |
|                     | Time (sec)  | 45            | 45       | 45       | 45    |
| Bake                | Temp. (°C)  | 170           | 170      | 170      | 170   |
|                     | Time (min)  | 1.5           | 1.5      | 1.5      | 15    |
| Film thickness (nm) |             | 536.3         | 270.3    | 287.5    | 244.8 |

\*Two different spin-on glass products were used. 315F and 21F indicate different part numbers for SOGs from Filmtronics Inc.

†PMMA solutions were diluted in anisole to make 4% PMMA solutions.

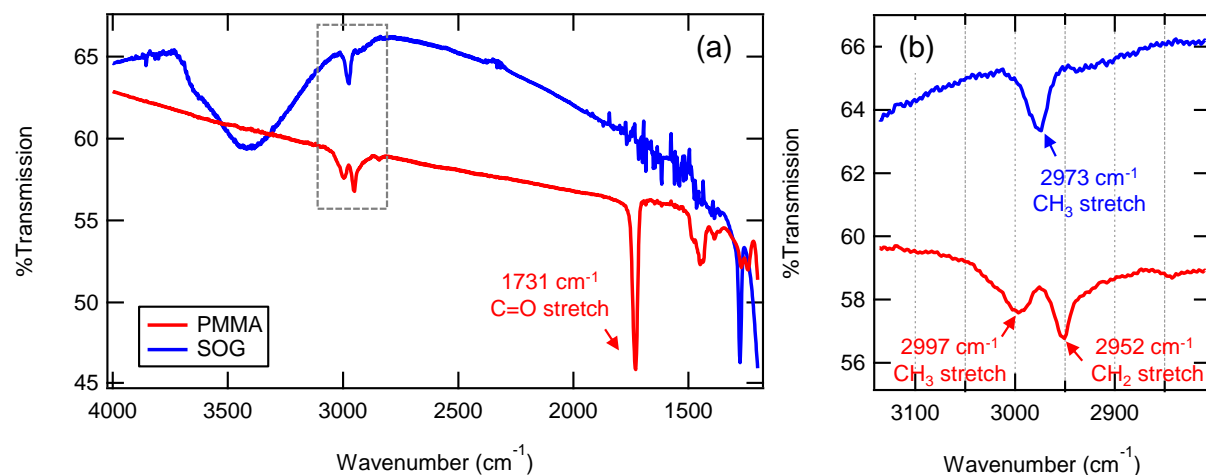


**Figure S1.** FTIR transmission spectrum of a bare PMMA and SOG film. (a) Each PMMA (thickness = 245 nm; red) and SOG (thickness = 568 nm; blue) film was prepared on metal-free silicon substrates. The transmission dip at 1731  $\text{cm}^{-1}$  in (a) corresponds to the carbonyl band of PMMA and those at 2997 and 2952  $\text{cm}^{-1}$  in (b) to the C-H bond stretching vibrations of the  $-\text{CH}_3$  and  $-\text{CH}_2$  groups, respectively. The SOG film exhibits the transmission dip at 2973  $\text{cm}^{-1}$  due to the symmetric  $\text{CH}_3$  vibration mode.

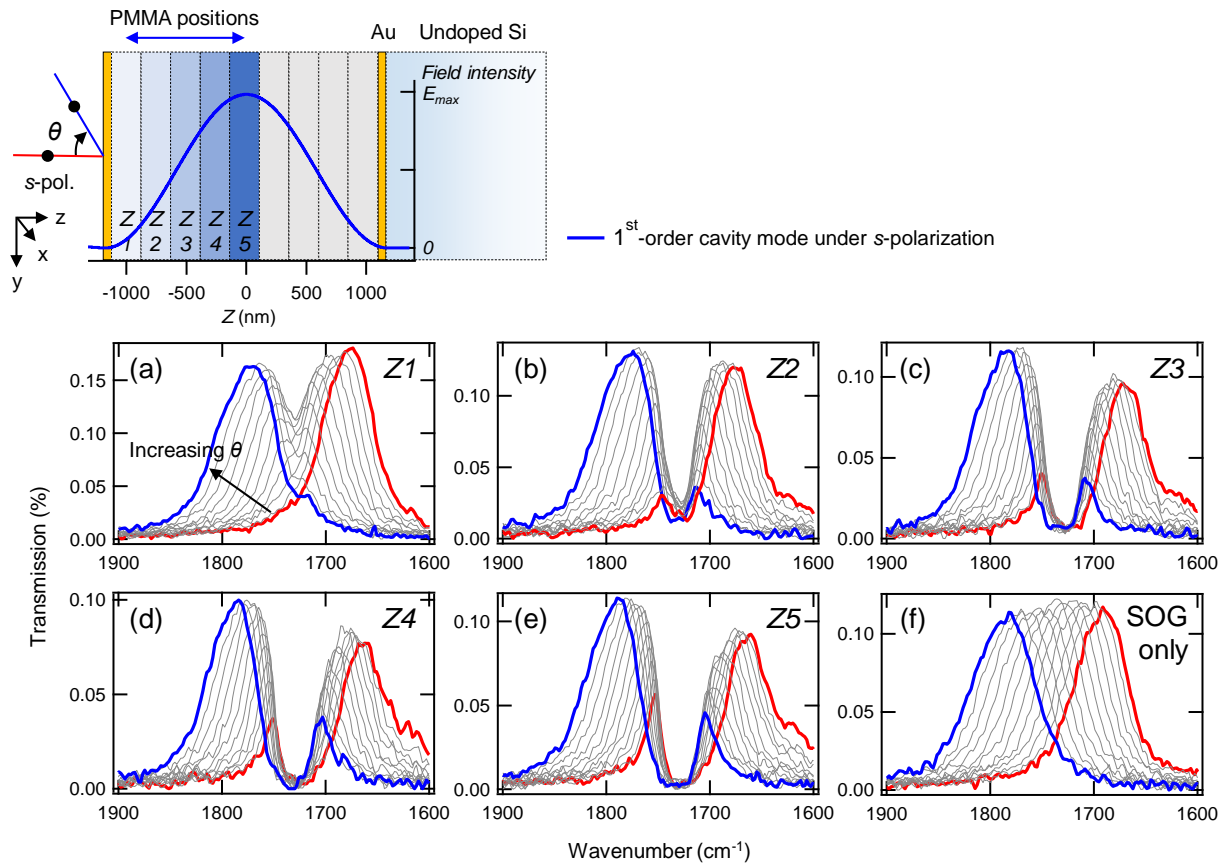


**Figure S2.** FTIR transmission spectra of Fabry-Perot cavities with variable PMMA locations within the cavity under s-polarization. Cavities containing a slab of PMMA film at different locations of Z1 – Z5 showed splittings in their transmission spectra as a result of coherent coupling between molecular vibrations and optical cavity modes (a-e). On the other hand, a control Fabry-Perot cavity that is free of PMMA but is entirely filled with SOG showed transmission spectra with no splitting in the same spectral range of 1600 – 1900  $\text{cm}^{-1}$  (f). FTIR transmission spectra were taken at varying angles of incident light ( $\theta$ ) to sweep through the carbonyl stretching band of PMMA centered at 1731  $\text{cm}^{-1}$ . Spectra with increasing  $\theta$  are shown from red to blue spectrum with 1° increment.

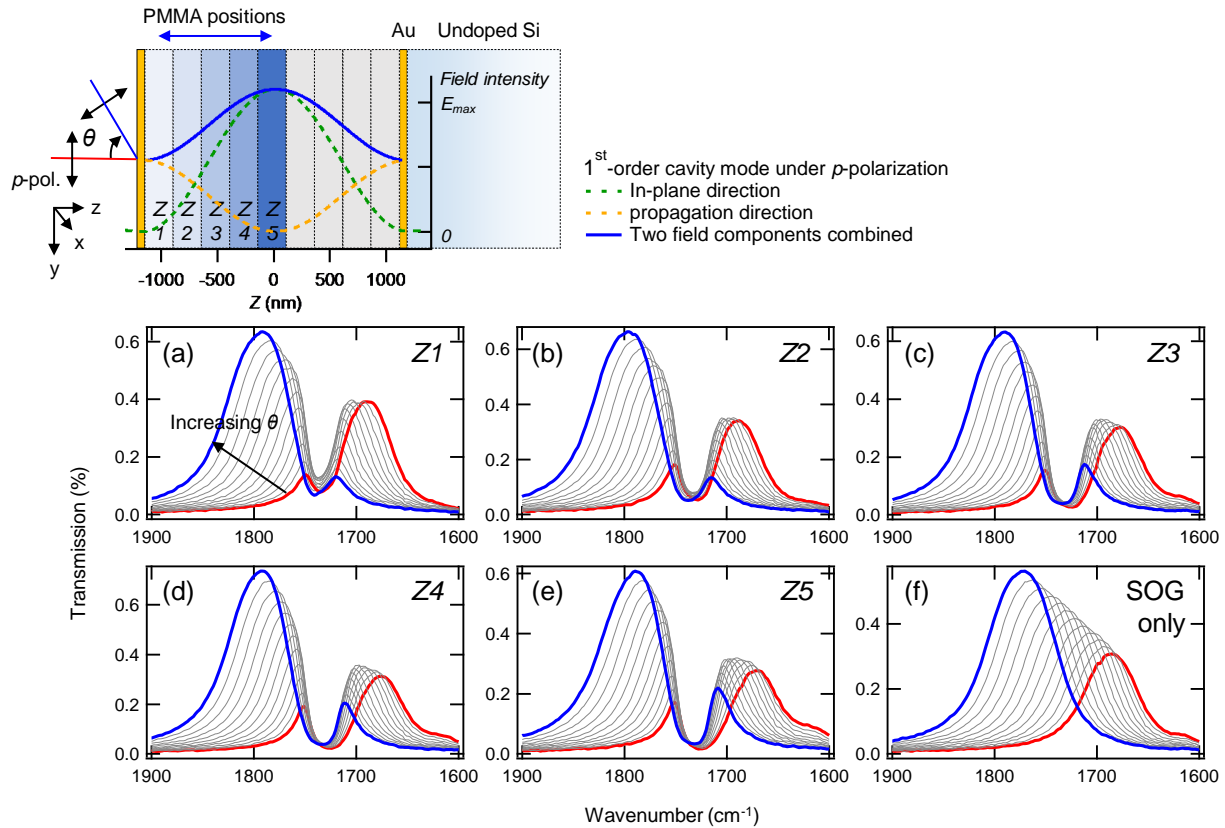


**Figure S3.** FTIR transmission spectra of Fabry-Perot cavities with variable PMMA locations within the cavity under  $p$ -polarization. Cavities containing a slab of PMMA film at different locations of Z1 – Z5 showed splittings in their transmission spectra as a result of coherent coupling between molecular vibrations and optical cavity modes (a-e). On the other hand, a control Fabry-Perot cavity that is free of PMMA but is entirely filled with SOG showed transmission spectra with no splitting in the same spectral range of 1600 – 1900  $\text{cm}^{-1}$  (f). FTIR transmission spectra were taken at varying angles of incident light ( $\theta$ ) to sweep through the carbonyl stretching band of PMMA centered at 1731  $\text{cm}^{-1}$ . Spectra with increasing  $\theta$  are shown from red to blue spectrum with  $1^\circ$  increment.

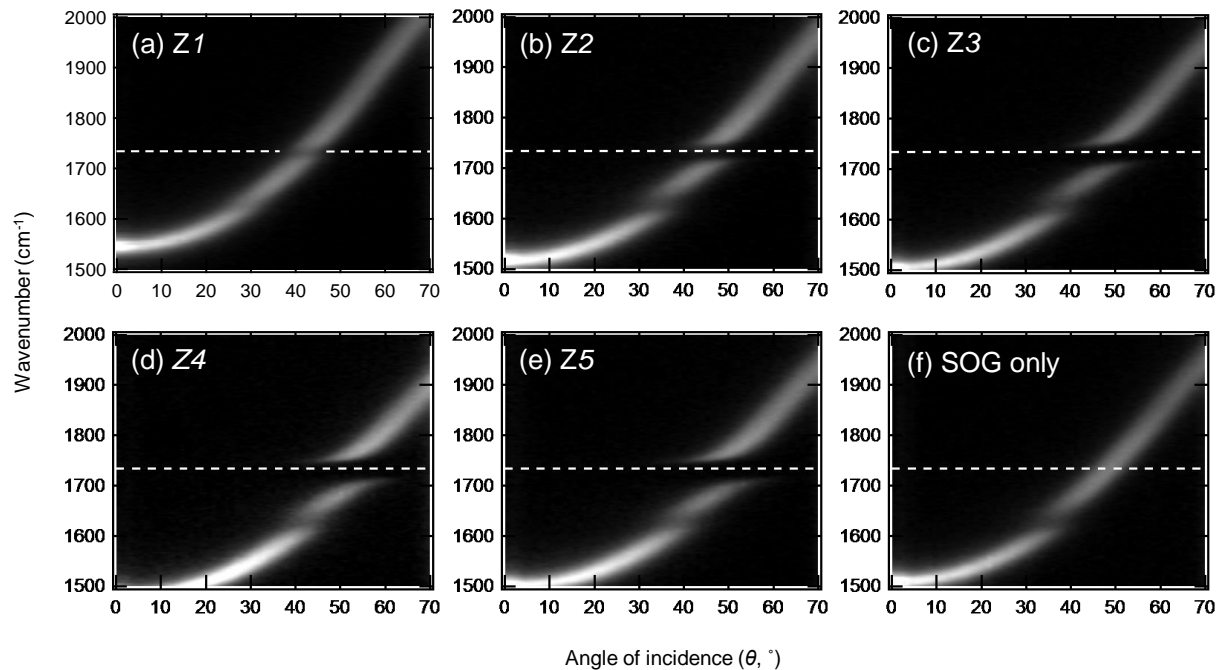


**Figure S4.** Angular dispersion curves of Fabry-Perot cavities with variable PMMA slab locations under s-polarization. Splittings between the upper branch (UB) and lower branch (LB) are clearly shown in each cavity (a – e) as an indication of vibrational strong coupling between the 1<sup>st</sup>-order cavity mode and the carbonyl stretching band of PMMA centered at 1731 cm<sup>-1</sup> (dashed white line). Splitting increases as the slab of PMMA film moves from the edge (a; Z1) to the center (e; Z5) of the cavity. Additional splitting shown at ~1630 cm<sup>-1</sup> is attributed to SOG as verified by a control cavity that is entirely filled with SOG without a PMMA slab (f). Note that in (f) there is no splitting resulting from the coupling between the optical cavity mode and the C=O stretching band of PMMA at 1731 cm<sup>-1</sup>.

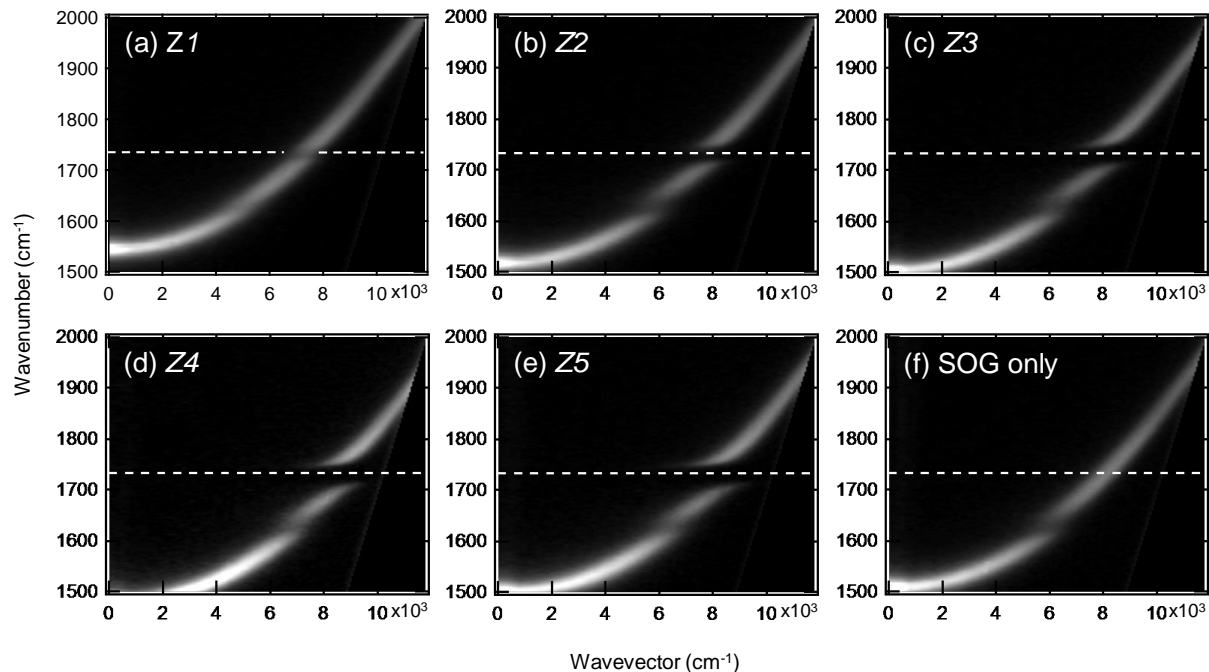


**Figure S5.** Cavity dispersion curves plotted versus in-plane wavevector for cavities with variable PMMA slab locations under s-polarization. Splitting between UB and LB centered at 1731 cm<sup>-1</sup> (C=O stretching band of PMMA; dashed white line) increases as the slab of PMMA film moves from the edge (a; Z1) to the center (e; Z5) of the cavity, indicating vibrational strong coupling between the 1<sup>st</sup>-order optical cavity mode and the molecular vibration mode. The control Fabry-Perot cavity with no PMMA slab (only SOG), however, showed no splitting resulted from the strong vibrational coupling at 1731 cm<sup>-1</sup> (f).

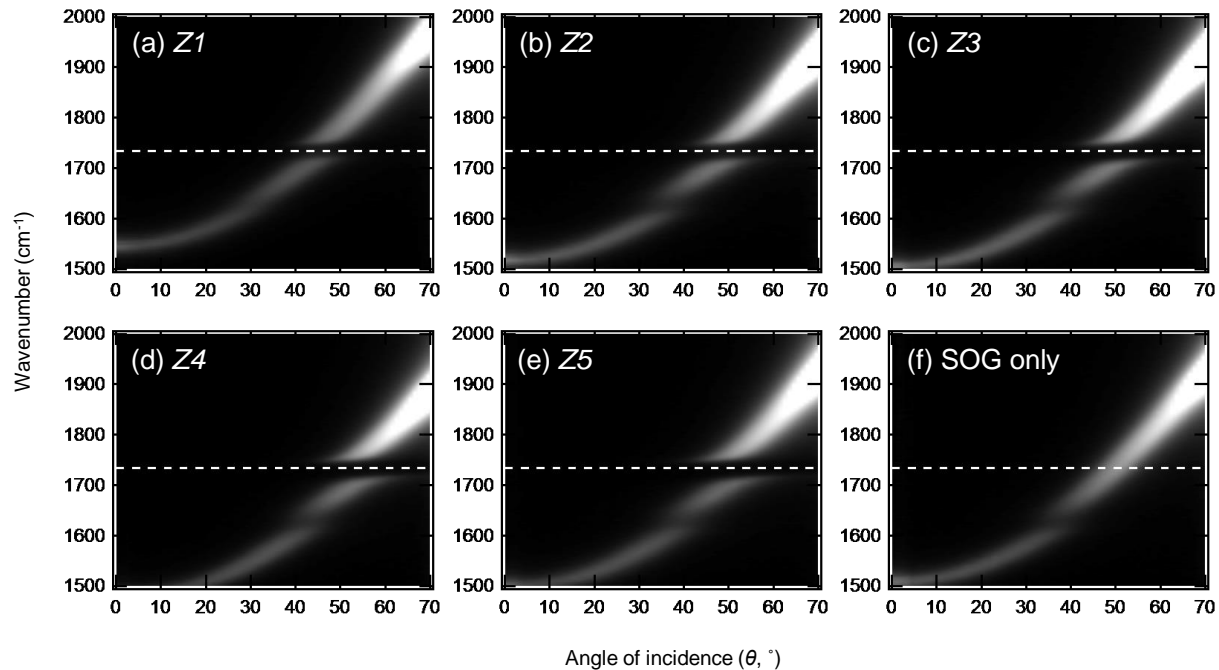


**Figure S6.** Angular dispersion curves of Fabry-Perot cavities with variable PMMA slab locations under *p*-polarization. Splittings between UB and LB are clearly shown in each cavity (a – e) as an indication of vibrational strong coupling between the 1<sup>st</sup>-order cavity mode and the carbonyl stretching band of PMMA centered at 1731 cm<sup>-1</sup> (dashed white line). Splitting increases as the slab of PMMA film moves from the edge (a; Z1) to the center (e; Z5) of the cavity. Additional splitting shown ~1630 cm<sup>-1</sup> is attributed to SOG as verified by a control cavity that was filled with SOG without a PMMA slab (f). Note that in (f) there is no splitting resulting from the coupling between the optical cavity mode and the C=O stretching band of PMMA at 1731 cm<sup>-1</sup>.

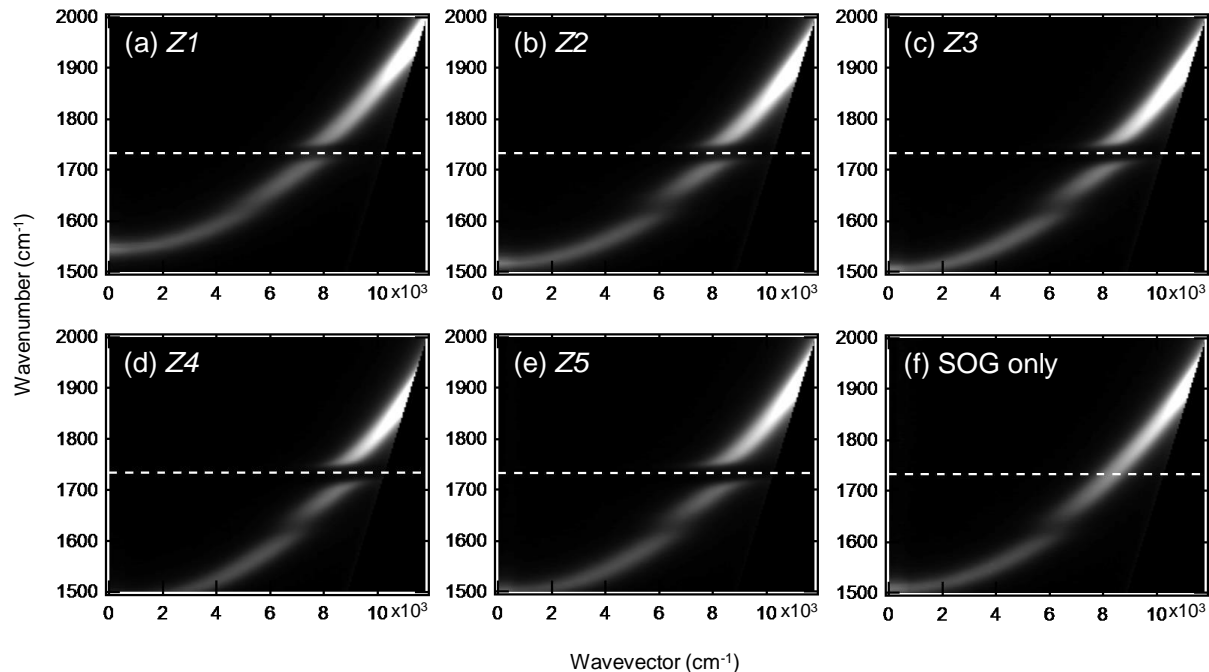


**Figure S7.** Cavity dispersion curves plotted versus in-plane wavevector for cavities with variable PMMA slab locations under  $p$ -polarization. Splitting between UB and LB centered at  $1731\text{ cm}^{-1}$  (C=O stretching band of PMMA; dashed white line) increases as the slab of PMMA film moves from the edge (a; Z1) to the center (e; Z5) of the cavity, indicating vibrational strong coupling between the 1<sup>st</sup>-order optical cavity mode and the molecular vibration mode. The control Fabry-Perot cavity with no PMMA slab (only SOG), however, showed no splitting resulted from the strong vibrational coupling at  $1731\text{ cm}^{-1}$  (f).

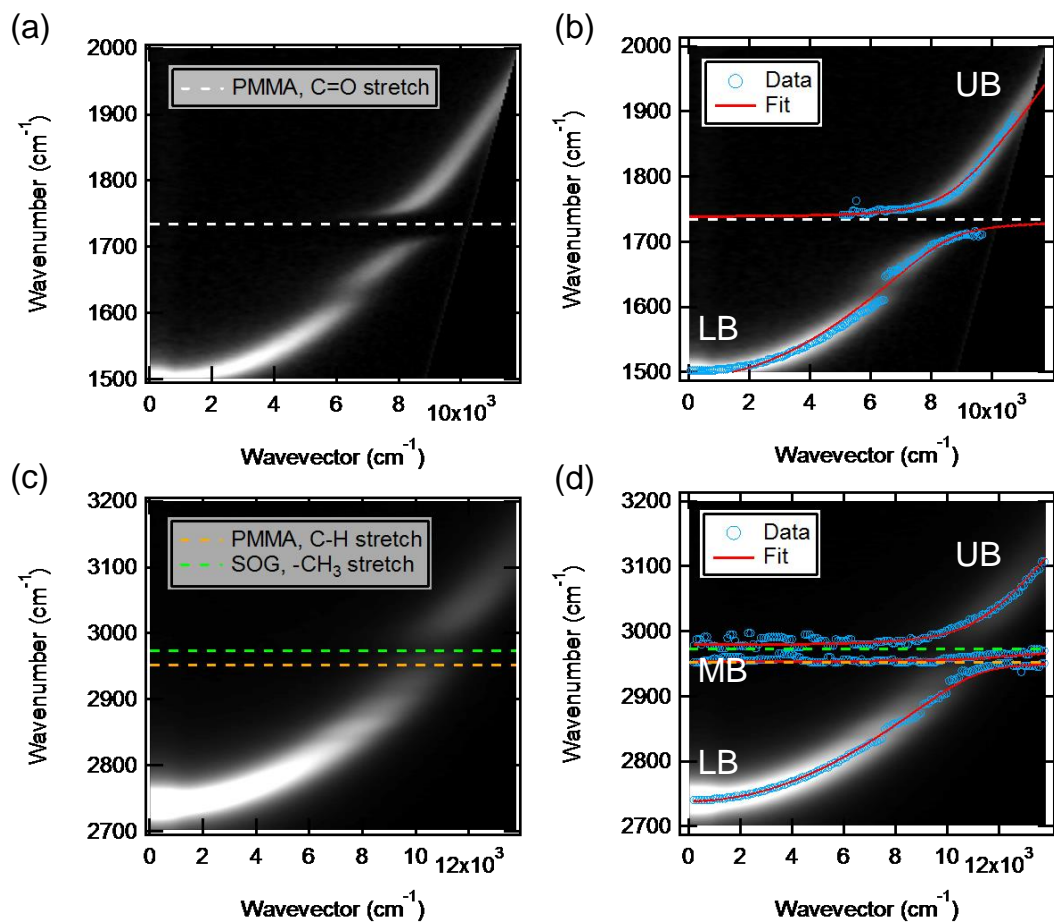


**Figure S8.** Data analysis for obtaining vacuum Rabi splitting values. Dispersion curves are shown for the coupling between the 1<sup>st</sup>-order cavity mode and PMMA C=O stretching band at 1731 cm<sup>-1</sup> (a, b) and that between the 2<sup>nd</sup>-order cavity mode and PMMA C-H stretching band at 2952 cm<sup>-1</sup> and the -CH<sub>3</sub> symmetric vibration mode of the SOG spacer at 2973 cm<sup>-1</sup> (c, d). Each vibrational mode was indicated in horizontal dashed lines. The upper and lower polariton dispersions were fitted to two (b) and three (d) coupled oscillator expressions (see the main text for equations), resulting in respective example fits (solid red curves). Note that two polaritonic states are shown as UB and LB in (b), whereas three polaritonic states are shown as UB, LB, and middle branch (MB) in (d).

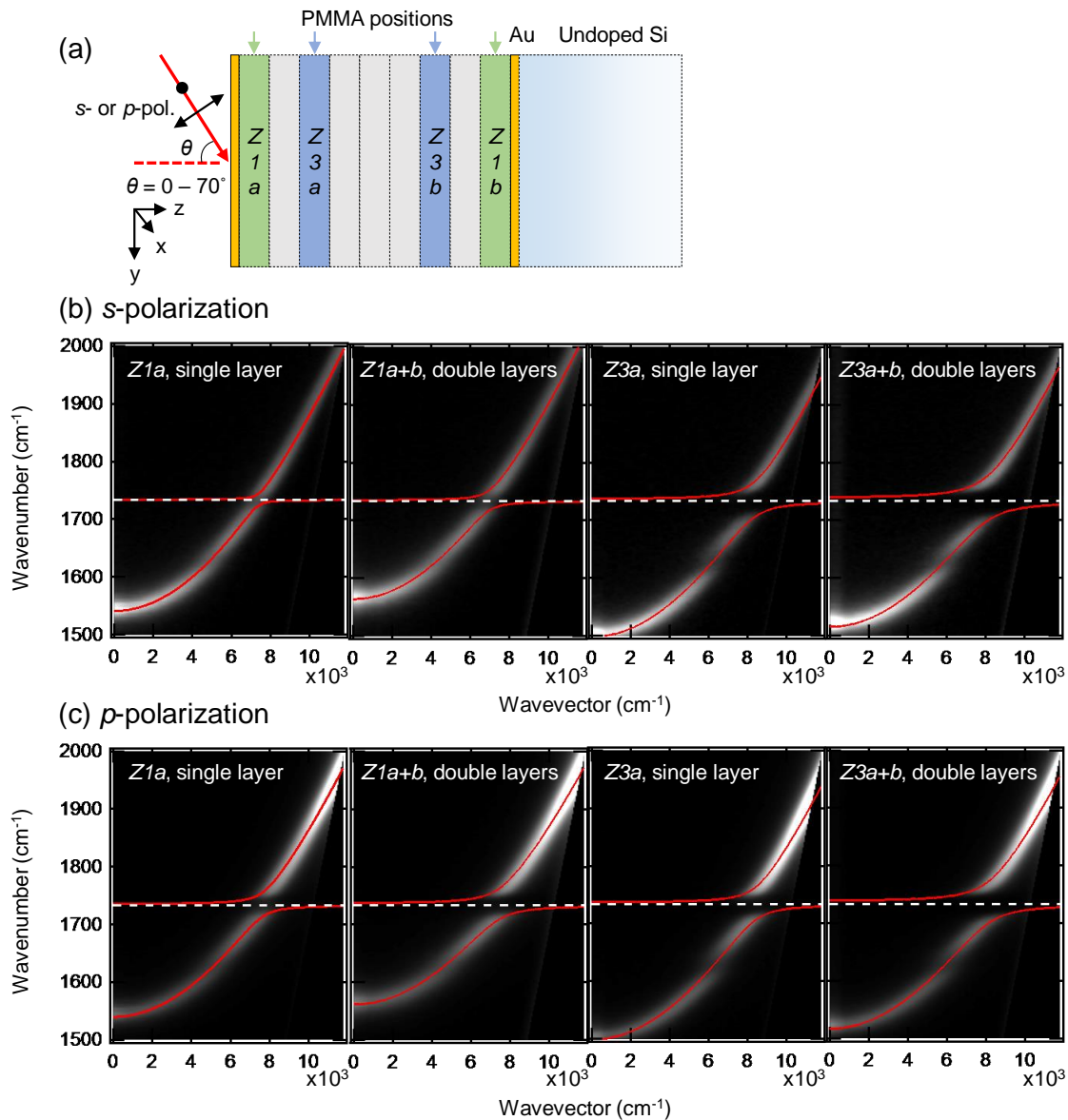


**Figure S9.** Dispersion curves of single and double PMMA layer cavities. (a) Schematic of the Fabry-Perot cavity consisting of one or two slab(s) of PMMA layer(s) at positions of either  $Z_{1a}$  and  $Z_{1b}$  (green) or  $Z_{3a}$  and  $Z_{3b}$  (blue). Dispersion curves of cavities having single or double layers of PMMA at each location of  $Z_1$  or  $Z_3$  for (b) s- and (c) p-polarization. Fitted curves of the upper and lower polariton dispersions to a two coupled oscillator expression are shown in solid red curves. Vacuum Rabi splittings increase in each case when the second remotely located molecular layer is added to the cavity.